Codeposition on Hot CVD Surfaces: Particle Dynamics and Deposit Roughness Interactions

Pushkar Tandon and Daniel E. Rosner
High Temperature Chemical Reaction Engineering Laboratory, Dept. of Chemical Engineering, Yale University, New Haven, CT 06520

To capture in a tractable manner essential coupling effects in CVD systems when particles generated in thermal boundary layers also deposit, a film theory was developed that predicts simultaneous vapor and particle deposition rates at a hot deposition surface. The codeposition rate prediction method also calculates for the first time the corresponding solid deposit roughness *using recently published results of particle-level simulations. For the numerical illustrations, the growth of $TiO_2(s)$ films by the codeposition of titanium tetra-isopropoxide vapor and film-nucleated/grown TiO_2 particles (generated in the thermal boundary layer) was considered. Experimental rate data for this system are available. The continuum and particle-level simulation methods provide: the interplay of vapor precursor kinetics, particle nucleation, growth, coagulation and diffusion in determining the complex "structure" of such multiphase chemically reacting boundary layers; wall deposition rates of both surviving vapors and film-nucleated particles; and the "self-consistent" microstructure (surface roughness) of the resulting solid deposit. Timely and tractable generalizations are discussed in the light of recent results for the transport properties and stability of "fractal-like" aggregated particles.*

Introduction

Chemical vapor deposition (CVD) processes are now widely used in industrial applications to produce ceramics (oxides, nitrides, carbides, etc.) and various composite materials from readily available vapor precursors (see, e.g., Ulrich, 1984; Biswas et al., 1989; Spear et al., 1990). These materials find applications in oxidation and/or wear-resistant coatings, solid-state electronic devices, and so forth. The commercial potential of such synthesis processes is often limited by low vapor deposition rates and high vapor precursor costs. Substantially increased deposition rates but complex deposit microstructures have been reported (see, e.g., Komiyama and Osawa, 1985; Komiyama et al., 1986, 1987; Hurt and Allendorf, 1991; Shimogaki and Komiyama, 1986) in systems where vapor deposition is "aided" by the *codeposition of particles*, either deliberately added to the mainstream or nucleated from gaseous precursors. At present, such "multiphase" CVD applications are beyond the scope of commercially available CVD-transport/reactor design software (Werner, 1993).

Okuyama et al. (1991) presented a model to predict deposition rates of SiO_2 particles nucleated during the CVD preparation of SiO_2 films from $SiCl_4$ and O_2 gases. Missing from their model, however, is simultaneous vapor transport to the surface, various levels of coupling between the vapor, suspended particle phase, and the nature of the deposit formed. Since there is still little understanding of the factors governing simultaneous vapor/particle/deposit interactions in such CVD boundary layers, we have developed and present here a simplified quiescent film theory to predict vapor and particle codeposition rates in such systems, together with the self-consistent deposit roughness. For our illustrative calculations, we consider the growth of $TiO_2(s)$ films on the hot surface by the codeposition of titanium tetra-isopropoxide (TTIP) vapor and $TiO_2(s)$ particles formed in the vapor-phase nonisothermal boundary layer from their gaseous precursors, a system for which net deposition rate data are available (Collins, 1994). In Figure 1 we show an impinging jet inductively heated "pedestal" flow reactor (Collins, 1994; Rosner et al., 1993) in which $TiO_2(s)$ film growth rates have been measured both in the absence and presence of reaction/par-

Correspondence concerning this article should be addressed to D. E. Rosner.

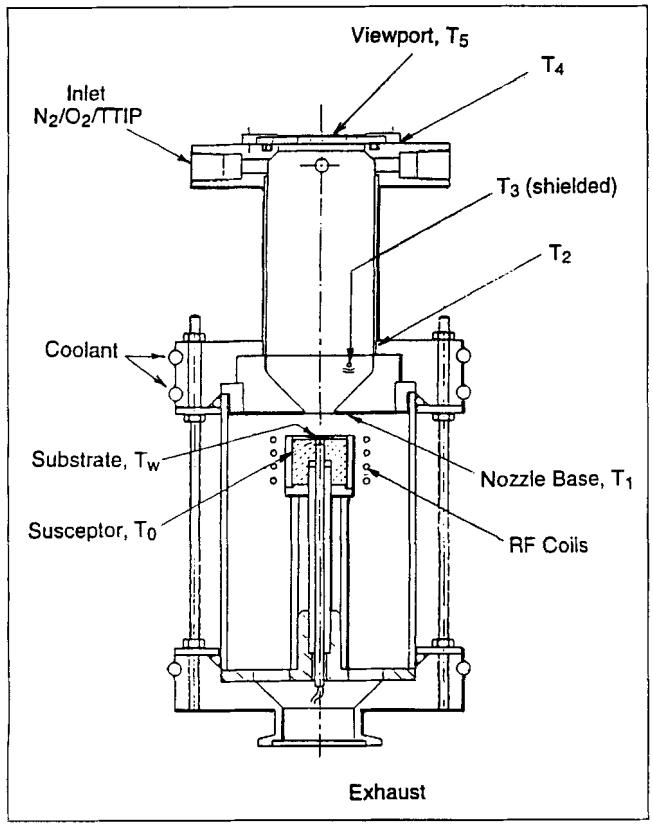

Figure 1. Axisymmetric impinging jet reactor.
Courtesy of Collins (1994).

ticle formation in the thermal boundary layer over the broad surface temperature interval: 600 to 1,400 K.

Figure 2 shows the various processes involved in the simultaneous vapor and particle deposition rates on a hot surface and various levels of coupling in situations where particles are generated within CVD boundary layers. In our present work, TTIP vapors are the trace "seed" species (with N_2 the main background gas) and diffuse through the nonisothermal boundary layer by Fickian- (concentration gradient-driven) and Ludwig-Soret (temperature gradient driven) diffusion. TTIP vapors reaching the surface undergo heterogeneous reaction leading to $TiO_2(s)$ film growth. However, at sufficiently high temperatures in the boundary layer, a fraction of these TTIP vapors pyrolize to generate TiO_2 monomers in the gas phase. These monomers are assumed to constitute pyrogenic nuclei that then grow by vapor scavenging and/or coagulation as they are transported by Brownian diffusion and thermophoresis near the hot surface. Our model predicts the steady-state vapor phase TTIP concentration profile, taking into account both first-order *homogeneous* and *heterogeneous* kinetics on the dispersed particulate surfaces (Castillo and Rosner, 1996; Okuyama et al., 1990) (in view of our overall purpose, the full set of "elementary" chemical reactions, which generally involves many arguable intermediate species and steps, is modeled as an overall, single-step-irreversible reaction in which the reagent is consumed following an Arrhenius-type first-order reaction-rate law). The titania local particle-size distribution (PSD) and corresponding local number density (N_p) in the boundary layer has been calculated by solving the coupled population balance equation (PBE), including diffusion (Brownian and thermophoretic), Brownian coagulation, growth, and nucleation terms. Thus, particles generated in the gas phase act as the local "pseudo-homogeneous" sink for TTIP vapors by CVD on their surfaces. Using an iterative scheme, we calculate vapor and particle deposition rates after self-consistent vapor-phase concentration profiles and particle number density and size distributions have been evaluated.

Castillo and Rosner (1996) have recently demonstrated and exploited the existence of a *chemical sublayer* (CSL) within the ordinary diffusional boundary layer, adjacent to the hot CVD surface for chemical systems characterized by high homogeneous activation energy. As an extension of their hypothesis, we also investigate the structure of "reaction–nucleation–coagulation" sublayer adjacent to the hot surface in the presence of suspended particles. Since their model predicts that most of the homogeneous chemistry is restricted to the chemical sublayer, we assume here that the particle nucleation and coagulation are likewise limited to this sublayer adjacent to the hot surface. The particles generated/coagulated in this sublayer are then carried through the outer boundary layer via the mechanisms of Brownian and thermophoretic diffusion, while a calculated fraction of these pyrogenic particles diffuse toward the hot surface. As illustrated in the third section, the results of our sublayer analysis are in reasonable agreement with those from a more complete analysis of the entire boundary layer.

Preliminary particle level simulation methods of Hurt and Allendorf (1991) have shown that in codeposition systems, *deposit roughness* is sensitive to the ratio of particle deposition rate to vapor deposition rate, which they considered to be a specified input parameter. But in systems where the particles are themselves generated within the boundary layer, this "ratio" is not known *a priori* and is itself a function of deposit roughness. The associated roughness of the deposit alters the rate of heterogeneous reaction by providing additional surface area for such reactions. This, in turn, alters the vapor phase concentration profile as well as the particle number density and size distribution in the adjacent boundary layer. In the section titled "Surface roughness and particle/vapor deposition rate" we show how the ratio of particle-to-vapor deposition rate is *coupled* with the roughness of such $TiO_2(s)$ films. Our methods (discussed in that section) to predict vapor and particle codeposition rates, taking into account this level of coupling, can be implemented more accurately when additional particle-level simulation results become available for polydisperse particle populations arriving nonballistically (Tassopoulos and Rosner, 1992, 1996; Tassopoulos, 1991).

Mathematical Model

Basic assumptions, simplifications, and idealizations

To capture the essential features of steady-state vapor precursor kinetics, vapor deposition and *particle* nucleation, coagulation, growth, diffusion, and deposition, without unduly complicating the analysis, we make the following *primary* assumptions:

A1. The "boundary layer" containing vapor concentration and temperature gradients is treated as a quiescent gas film, that is, "convection" normal to the surface is neglected. Con-

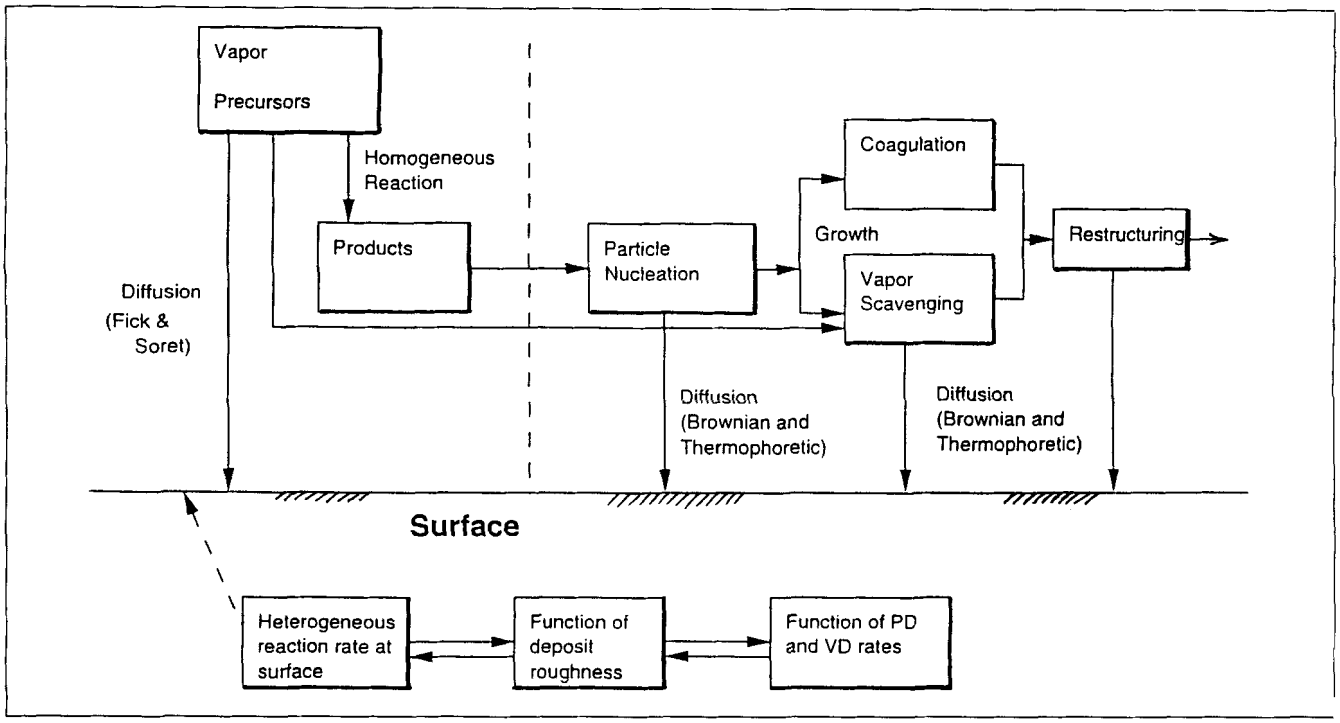

Figure 2. Participating processes in the case of simultaneous particle and vapor deposition ("codeposition") on hot surfaces.

centration and temperature gradients through the boundary layer are essentially perpendicular to the hot surface.

A2. The thickness of mass-transfer boundary layer is approximately equal to the thickness of the thermal boundary layer.

A3. All solid titanium dioxide to precipitate is formed by the thermal decomposition of TTIP(g) and starts out as TiO_2 monomers.

A4. The effective diameter of a TiO_2 monomer is assumed equal to the effective hard-sphere diameter of a TiO_2 vapor molecule.

A5. Temperature and particle number density are known at bulk and wall conditions. Moreover, vapor phase composition in the mainstream is also considered known.

A6. The physicochemical processes (deposition, chemical reaction, etc.) undergone by the dilute reacting species and the presence of particles found in the boundary layer do not appreciably affect the temperature field.

A7. The local coalescence rate of the coagulating particles is rapid enough to give rise to spherical particles assumed to be composed of a single component only (TiO_2). Thus, particle *volume* is the only required "*internal*" variable in solving the population balance equation.

The defense and/or generalizations of these idealizations/assumptions are discussed later, as well as criteria to define their approximate limits of validity. Several will be seen to be readily generalized to embrace more complex situations of inevitable practical interest. Secondary assumptions will be introduced as required in the course of our analysis.

Mathematical Model

Our simplified model deliberately avoids details that will unnecessarily complicate the analysis, while retaining the main physicochemical characteristics of coupled processes involving a vapor precursor and resulting pyrogenic seed particles. In this way insight can be provided on the *interplay* of the various vapor/particle and particle/particle processes occurring in the boundary layer, and at the rough vapor/deposition interface. Accordingly, a steady-state situation has been chosen with the simplest geometrical configuration, namely, a thin layer of gas to be confined between two parallel surfaces: the CVD surface located, at, say, $y = 0$, and the mainstream at $y = \delta_{BL}$, where δ_{BL} is the effective outer edge of the boundary layer. This geometrical configuration leads to a single independent spatial variable, y, that is, position in the direction normal to the CVD surface.

Temperature Field. The energy balance equation for a steady-state quiescent film with negligible contribution from gas-phase homogeneous reaction of the dilute TiO_2-precursor or the other physicochemical processes going on in the boundary layer simplifies to (see Rosner, 1986):

$$\mathrm{div}\{\dot{q}''\} = 0, \tag{1}$$

where the local heat flux $\dot{q}''$ has a y-component given by the Fourier law

$$\dot{q}''_y = k\left(-\frac{dT}{dy}\right). \tag{2}$$

Assuming a simple power-law temperature dependence for the vapor mixture thermal conductivity k (i.e., $k = k_0 T^{\epsilon}$, where, usually, $\frac{1}{2} \le \epsilon \le 1$, depending on the choice of the background gas) we immediately obtain the temperature distribution across the gas thermal layer in the simple form:

$$\frac{T^{\epsilon+1}}{\epsilon+1} = C_1 y + C_2. \tag{3}$$

With the temperatures at the two surfaces prescribed as $T = T_w$ at $y = 0$ and $T = T_e$ at $y = \delta_{BL}$, the constants of integration C_1 and C_2 are easily calculated to be

$$C_1 = \frac{(T_e^{\epsilon+1} - T_w^{\epsilon+1})}{(\epsilon+1)\cdot\delta_{BL}}; \qquad C_2 = \frac{T_w^{\epsilon+1}}{\epsilon+1}. \tag{4}$$

The thermal boundary layer thickness δ_{BL} is assumed here to be roughly equal to the mass-transfer boundary-layer thickness. For the configuration of Figure 1 we select δ_{BL} to be of the order (the effective thermal boundary-layer thickness has also been obtained by approximately equating the calculated surface mass flux to the observed mass flux in the diffusion controlled regime):

$$\delta_{BL} = \frac{d_{\text{jet}}}{Nu_h}. \tag{5}$$

Here Nu_h is the prevailing laminar heat-transfer coefficient (Nusselt number) and is well described as a function of impinging-jet Reynolds number, Re, and Prandtl number, Pr, as (Schlichting, 1979):

$$Nu_h = 0.98\cdot(Re)^{1/2}(Pr)^{0.371}. \tag{6}$$

The Reynolds number is defined in terms of jet diameter, d_{jet}, and jet velocity, U_{jet}, as

$$Re = \frac{U_{\text{jet}} d_{\text{jet}}}{(\mu/\rho)}. \tag{7}$$

The Reynolds number and the Prandtl number have been calculated at the arithmetic mean temperature in the film. The local transport and thermodynamic properties used here and in the following three subsections (specific heat, c_p; density, ρ; viscosity, μ; thermal conductivity, k; thermal diffusion factor, α; Fick diffusion coefficient, $D_{i\text{-mix}}$) have been estimated using the gas kinetic methods discussed in Rosner and Tandon (1991) and Gokoglu et al. (1984).

Vapor-Phase Concentration Profile. In the particular case that motivated this work, TTIP is the trace vapor species with N_2 as the background gas. TTIP(g) diffuses through the gas toward the hot wall, where it undergoes a heterogeneous chemical reaction with the product TiO_2(s) being deposited there. On the other hand, this precursor vapor also undergoes chemical reaction in the gas phase at the local (mass-) *rate of consumption*, $-\dot{r}'''_{i,\text{eff}}$ per unit time and volume. The local rate of consumption of TTIP, $\dot{r}'''_{i,\text{eff}}$, is composed of two contributions, one from true homogeneous reactions and one from CVD reactions on the surfaces of suspended particles. Under steady-state conditions, for a quiescent film (or, more generally, a film within which $\rho \boldsymbol{v}\cdot\boldsymbol{grad}\ \omega_i$ is small compared to the indicated terms in Eq. 8), the mass balance equation for a trace species i (here TTIP) can be formally written

$$0 = -\text{div}\{\boldsymbol{j}''_i\} + \dot{r}'''_{i,\text{eff}}. \tag{8}$$

For simplicity, the full set of "elementary" homogeneous chemical reactions leading from TTIP pyrolysis to TiO_2-monomer production, which generally involves many intermediate species and "steps," has been modeled as an overall, single-step irreversible reaction:

$$\text{Ti}(OC_3H_7)_4 \rightarrow TiO_2 + 4C_3H_6 + 2H_2O. \tag{9}$$

Accordingly, the local consumption of reagent i (here TTIP) is taken to be a first-order Arrhenius-type reaction law:

$$-\dot{r}'''_{i,\text{eff}} = k_{\text{hom}}\cdot(\rho\omega_i) = [A_{\text{hom}}\exp(-E_{\text{hom}}/(RT))](\rho\omega_i), \tag{10}$$

where ω_i is the mass fraction of the dilute reagent species. For TTIP, the preexponent A_{hom} and activation energy E_{hom} have been reported as (Okuyama et al., 1990; Castillo and Rosner, 1996):

$$A_{\text{hom}} = 3.96\times10^5\ \text{s}^{-1}; \qquad E_{\text{hom}} = 7.05\times10^4\ \text{J mol}^{-1}. \tag{11}$$

We postpone to the section on vapor scavenging an account of our treatment of the vapor scavenging (by suspended particles) contribution to the effective local TTIP consumption rate, $\dot{r}'''_{i,\text{eff}}$.

Because of high-temperature gradients in CVD systems, the diffusive transport flux j''_i of the dilute reagent species i comprises contributions from both Fickian- (concentration gradient) and Ludwig-Soret (temperature gradient) diffusion (Rosner, 1980, 1988), that is, for the y-component:

$$j''_{i,y} = -\rho D_{i\text{-mix}}\cdot\left[\frac{d\omega_i}{dy} + \frac{\alpha_i\omega_i}{T}\frac{dT}{dy}\right]. \tag{12}$$
"Fick" "Ludwig-Soret"

where $D_{i\text{-mix}}$ is the trace species pseudobinary Fick diffusion coefficient and α_i is the corresponding dimensionless *thermal diffusion factor*, estimated (using methods described in Rosner et al., 1979; Gokoglu et al., 1984) as

$$\alpha_{\text{TTIP/N}_2} = 0.301\left(1 - \frac{485}{T}\right). \tag{13}$$

Undecomposed TTIP vapors reaching the hot wall are assumed to undergo *heterogeneous* reaction at this surface, with the rate of reactant mass consumption (per unit surface area and time) given by

$$-\dot{r}''_w = A_{\text{het}}\,\rho\omega_w\cdot\exp[-E_{\text{het}}/RT_w], \tag{14}$$

where A_{het} and E_{het} are, thus, the *heterogeneous* preexponential factor and activation energy, respectively. They have been estimated from the observed surface reaction rates of TTIP to TiO_2 as (Collins, 1994; Castillo and Rosner, 1995)

$$A_{\text{het}} = 0.52\times10^{10}\ \text{cm s}^{-1}; \qquad E_{\text{het}} = 120\ \text{kJ}\cdot\text{mol}^{-1}. \tag{15}$$

The second-order ODE, Eq. 8, is solved for the vapor concentration profile using a finite-difference method with the following boundary conditions:

$$\omega = \omega_e \qquad @\ y = \delta_{BL} \qquad (16a)$$

$$j''_{i,w} = \dot{r}''_{i,w,\text{het}} = (\dot{r}''_{i,w})_{\text{smooth}} \cdot (a''/a''_0) \qquad @\ y = 0 \qquad (16b)$$

where (a''/a''_0) is the extra interfacial area provided for the heterogeneous reaction because of the roughness of the "granular" deposit (see the section titled "Surface roughness and particle/vapor deposition rate"). The whole boundary layer is divided into P number of nodes (node 0 is the outer edge of the boundary layer while $P+1$ corresponds to the wall and h is the distance between successive nodes). The second-order ODE, Eq. 8, is discretized using a finite-differencing technique and is satisfied at each node m ($m = 1,\ldots, P$) in the boundary layer. Moreover, the boundary conditions specified by Eq. 16 are satisfied. Thus, we have a set of $(P+1)$ linear equations in $P+1$ variables (TTIP mass fraction at each of the P nodes and TTIP mass fraction at the wall) that are solved to obtain the steady-state TTIP vapor concentration profile in the boundary layer. The vapor flux at the wall is estimated once the concentration profile is obtained.

Particle Number Density and Size Distribution. The dilute reagent undergoing reaction in the gas phase yields products that may nucleate and ultimately form solid particles "suspended" in the gas phase. We consider that all TiO_2 formed locally from the thermal decomposition of TTIP locally appears as TiO_2 monomers. The monomers generated in the gas phase in turn coagulate to form larger particles. For simplicity, the coalescence rate of the coagulating particles is considered rapid enough to give rise to spherical particles (see the discussion in the fourth and fifth sections). The particles thus generated in the gas phase migrate (Brownian and thermophoretically) through the gaseous boundary layer near the hot surface. To predict the local particle number density and size distribution in the boundary layer, a local population balance equation (PBE) is formulated and solved. The PBE under steady-state conditions for a quiescent film is the local balance of diffusion, coagulation, nucleation, and growth terms, or, symbolically,

$$0 = \text{Diffusion term} + \text{coagulation term} + \text{nucleation term} + \text{growth term}. \qquad (17)$$

Since we assume that all TiO_2 formed from thermal decomposition of TTIP locally becomes titanium dioxide monomers, the nucleation term (number of monomers generated per unit time and volume) is estimated from homogeneous kinetics data for TTIP vapor pyrolysis. The corresponding particle nucleation term B_0 can then be estimated as

$$B_0 = \frac{\dot{r}'''_{\text{TiO}_2,\text{hom}}}{\rho_{\text{TiO}_2} \cdot v_1}, \qquad (18)$$

where ρ_{TiO_2} (≈ 4.2 g/cm^3) is the mass density of each TiO_2 particle and v_1 is the monomer volume (assumed to be equal to that of a single TiO_2 molecule, or about 0.019 (nm)^3). The nucleation term in the PBE can then be formally written:

$$B_0 \delta\{v - v_1\}, \qquad (19)$$

where $\delta\{\ \}$ is the Dirac delta function.

The net coagulation term contains two sets of contributions: the first set consists of birth of particles of size v by coagulation of particles with volumes smaller than v. The second set is associated with the death of particles because particles of size v coagulate to form larger particles. The net rate of production of particles of size u is then given as

$$\frac{1}{2}\sum_{w=1}^{u} \beta\{u-w,w\} \cdot N\{u-w\} \cdot N\{w\} - N\{u\} \cdot \sum_{w=1}^{\infty} \beta\{u,w\} N\{w\}, \qquad (20)$$

where $\beta\{u, w\}$ is the collision rate constant between particles of volumes u and w. The coagulation terms in the general population balance have been modeled using a numerical method suggested in Hounslow et al. (1988). The size spectrum is divided into M sections in a geometric series such that the smallest size in the ith section has 2^i monomers and the largest size has 2^{i+1} monomers. The rate of production per unit volume at location y of particles in ith section because of coagulation is

$$N_{i-1}\{y\} \cdot \sum_{j=1}^{i-2} 2^{j-i+1} \beta_{i-1,j}\{y\} N_j\{y\} + \frac{1}{2}\beta_{i-1,i-1}\{y\} N^2_{i-1}\{y\} - N_i\{y\} \cdot \sum_{j=1}^{i-1} 2^{j-i} \beta_{i,j}\{y\} N_j\{y\} - N_i\{y\} \cdot \sum_{j=i}^{\infty} \beta_{i,j}\{y\} N_j\{y\}, \qquad (21)$$

where $N_i\{y\}$ is the number density of particles in the ith interval at location y, and $\beta_{i,j}\{y\}$ is the collision frequency of spherical particles in the ith and jth intervals at location y. Considering all collisions to be in the free-molecular regime, the particle–particle collision rate constant $\beta_{i,j}$ is calculated for the arithmetic mean volume of particles in ith and jth interval, and may be written (Friedlander, 1977)

$$\beta_{i,j} = \left(\frac{3}{4\pi}\right)^{1/6} \cdot \left(\frac{6k_B T}{\rho_p}\right)^{1/2} \cdot \left(\frac{1}{v_{av,i}} + \frac{1}{v_{av,j}}\right)^{1/2} \cdot \left(v_{av,i}^{1/3} + v_{av,j}^{1/3}\right)^2. \qquad (22)$$

The divergence of the local diffusion flux vector in the PBE includes contributions from Brownian and thermophoretic diffusion, that is

$$\frac{d}{dy}\left[\rho D_{SE,i}\left(\frac{d(N_i/\rho)}{dy} + \frac{\alpha_{Tp,i}(N_i/\rho)}{T}\frac{dT}{dy}\right)\right]. \qquad (23)$$

Here, $D_{SE,i}$, Brownian diffusion coefficient of particles in the ith section (this has again been calculated for the arithmetic mean volume in the ith interval) is calculated as (Rosner, 1986)

$$D_{SE,i} = \frac{k_B T}{3\pi\mu d_i / C_i}, \tag{24}$$

where d_i is the average diameter of particles in the ith interval, and C_i, the Stokes–Cunningham slip correction factor, is a function of the Knudsen number Kn (= mean free path/d_i) taken here to be

$$C_i \cong 1 + Kn\left[2.52 + 0.8\cdot\exp\left(-\frac{0.55}{Kn}\right)\right]. \tag{25}$$

The thermophoretic factor, $\alpha_{Tp,i}$, in the free-molecular regime can be written (Waldmann and Schmitt, 1966; Garcia-Ybarra and Rosner, 1989; Gomez and Rosner, 1993; Rosner et al., 1992) as

$$\alpha_{Tp,i} = \left(\frac{3}{4}\right)\cdot\left[1+\left(\frac{\pi\alpha_{\text{mom}}}{8}\right)\right]^{-1}\cdot\frac{\nu}{D_{SE,i}}, \tag{26}$$

where α_{mom} is the tangential *momentum* accommodation coefficient and ($\nu \equiv \mu/\rho$) is the momentum diffusivity of the local gas mixture. The specified particle number density in the bulk and at the wall serve as the required boundary conditions. For each size class i the *particle* number density at the wall and in the mainstream are considered to vanish (assuming no particles in the mainstream and perfect capture at wall), that is,

$$N_i = 0 \qquad @\ y = 0 \quad \text{and} \quad y = \delta_{BL} \qquad (i = 1,2,\ldots, M). \tag{27}$$

We postpone to the following subsection an account of our treatment of the growth term (as a result of vapor scavenging by suspended particles) in the PBE (Eq. 17). The finite-difference discretized version of the PBE (Eq. 17) is satisfied at each of the nodes m ($m = 1,\ldots, P$) for each size class i ($i = 1,\ldots, M$). Thus the population balance for particles in the ith size class interval at the node m can be approximated as

$$\begin{aligned} F(i,m) = {} & D_{SE,i}\left[\frac{N_{i,m-1} - 2N_{i,m} + N_{i,m+1}}{h^2}\right] + \frac{D_{SE,i}\alpha_{TP,i}}{T_i} \\ & \times \frac{(N_{i,m-1} - N_{i,m+1})}{2h}\cdot\frac{dT}{dy} + D_{SE,i}\alpha_{TP,i}N_{i,m}\cdot\frac{d}{dy}\left(\frac{1}{T}\frac{dT}{dy}\right) \\ & + B_{0-i,m} + N_{i-1,m}\sum_{j=1}^{i-2} 2^{j-i+1}\cdot\beta_{i-1,j,m}N_{j,m} \\ & + \frac{1}{2}\cdot\beta_{i-1,i-1,m}N_{i-1,m}^2 - N_{i,m}\sum_{j=1}^{i-1} 2^{j-i}\cdot\beta_{i,j,m}\cdot N_{j,m} \\ & - N_{i,m}\sum_{j=1}^{M}\beta_{i,j,m}\cdot N_{j,m} = 0. \end{aligned} \tag{28}$$

We therefore encounter ($M \times P$) nonlinear equations in ($M \times P$) ($N_{i,m}$; $i = 1,\ldots, M$; $m = 1,\ldots, P$) variables that have been solved iteratively using the Newtonian–Raphson method. In our present simulations (the third section) the values $P = 30$ and $M = 15$ were found to be adequate, and further increases in the values of P and Q did not appreciably affect the results. The local particle number density and particle-size distribution are required to estimate the particle number flux at the wall.

Vapor scavenging by suspended particulate matter

In general the simultaneous presence of suspended particulate matter within the boundary layer leads to scavenging of vapor by particles, thereby influencing local vapor concentrations, particle nucleation rate, particle-size distribution, and vapor/particle deposition rate (Castillo and Rosner, 1988). For scavenging of the reactant vapor by suspended particles of local number density $N\{y\}$ and local average particle radius, $\overline{r_p\{y\}}$ [where $N\{y\} = \sum_{i=1}^{M} N_i\{y\}$ and $N\{y\}\overline{r_p\{y\}}^2 = \sum_{i=1}^{M} N_i\{y\}\cdot r_i^2$], the ratio of the local heterogeneous (on the surface of the suspended particles) reaction rate constant to the local homogeneous reaction rate in the free-molecular regime is defined as

$$C_{\text{part}}\{y\} = \frac{4\pi\left(\frac{\bar{c}\cdot\epsilon_w}{4}\right)}{k_{\text{hom}}(y)}\cdot\sum_{i=1}^{M}[N_i\{y\}r_i^2\{y\}]\left(1+\frac{\sigma_{\text{TTIP}}}{2r_{av,i}}\right)^2 \cdot\left(1+\frac{M_{\text{TTIP}}}{(v_{av,i}/v_1)M_{\text{TiO}_2}}\right)^{1/2}, \tag{29}$$

where ϵ_w is the heterogeneous reaction probability for TTIP ($\epsilon_w < 1$), assumed here to be particle-size-independent. The last two factors inside the summation on the righthand side of Eq. 29 takes into account the fact that the smallest particles are undergoing appreciable Brownian motion [NB: in the absence of such Brownian motion, we recover the familiar expression $k''_{\text{het}} = (\bar{c}\cdot\epsilon_w/4)$]. The effective consumption rate of TTIP, r''_{eff}, (in Eq. 8) besides the contribution from the homogeneous reaction rate in the boundary layer (given by Eq. 10) will also have a contribution from the heterogeneous rate at the surface of the suspended particles, that is,

$$\begin{aligned} \dot{r}'''_{\text{eff},i}\{y\} &= \dot{r}'''_{\text{hom},i}\{y\} + \dot{r}'''_{\text{het},i}\{y\} \\ &= k_{\text{hom}}\{y\}\cdot(1 + C_{\text{part}}\{y\})\cdot(\rho\omega_i\{y\}). \end{aligned} \tag{30}$$

As a result, the corresponding rate of linear growth of particles because of vapor scavenging is estimated to be

$$G_i\{r\} = \frac{\left(\frac{\bar{c}\cdot\epsilon_w}{4}\right)\rho\omega_i\cdot M_{\text{TiO}_2}}{\rho_{\text{TiO}_2}\cdot M_{\text{TTIP}}}\cdot\left(1+\frac{\sigma_{\text{TTIP}}}{2r_{av,i}}\right)^2 \cdot\left(1+\frac{M_{\text{TTIP}}}{(v_{av,i}/v_1)M_{\text{TiO}_2}}\right)^{1/2}. \tag{31}$$

Because of this growth term an additional contribution will appear on the righthand side of population balance equation, Eq. 17. The growth term has been modeled using methods discussed in Hounslow et al. (1988) and is given as

$$\left(\frac{dN_i}{dt}\right)_{\text{growth}} = \frac{2G_i\{r\}}{d_i}(aN_{i-1} + bN_i + cN_{i+1}), \quad (32)$$

where

$$a = -c = \frac{2r}{(1+r)\cdot(r^2-1)} \quad \text{and} \quad b = \frac{2}{(1+r)},$$

where $r = \sqrt[3]{2}$. The reaction probability, ϵ_w, is estimated using our deposition rate data in the heterogeneous reaction-controlled regime (600 K $\leq T_w \leq$ 700 K) and is calculated as

$$\epsilon_w = \text{Min}\{5\times10^5\cdot\exp(-E_{\text{het}}/RT_w), 1\}. \quad (33)$$

Since values of $N_i\{y\}$ required to calculate C_{part} in Eq. 29 are not known *a priori*, our methods (in the section on the mathematical model) are used iteratively to include the vapor-scavenging effect by suspended particles. Here local particle-size distribution (PSD) and number density ($N\{y\}$) are assumed and new values of PSD and $N\{y\}$ are estimated using our film model. These procedures are iterated until the computed values are in reasonable agreement with (e.g., within 1%) the assumed values.

Results and Discussion

Principal results

Figure 2 summarizes the various processes involved in the simultaneous vapor and particle deposition on a hot surface and various levels of coupling in situations where particles are generated in CVD boundary layers. In Figure 1 is shown the axisymmetric impinging jet, inductively heated pedestal flow chemical vapor deposition reactor (Collins, 1994; Rosner et al., 1993) in which growth rates of TiO_2(s) films by codeposition of TTIP vapors and TiO_2(s) particles (the system we have chosen to illustrate our methods discussed in the previous section) have been measured over the broad surface temperature interval: 600 to 1,400 K. The experiments and our present numerical simulations were carried out for the following conditions: $\omega_e = 2.48\times10^{-3}$ (at 1,200 K), $d_{\text{jet}} = 1.3$ mm and 5.16 L/min. We solve the energy balance and species mass balance equation to obtain the temperature and TTIP vapor phase concentration profile in the boundary layer. These are shown in Figure 3 for the prescribed wall and mainstream temperatures as $T_w = 1{,}200$ K and $T_e = 380$ K. Besides the depletion of TTIP as a result of the homogeneous pyrolysis reaction, there is vapor scavenging by suspended particles. The resulting local particle number density is shown in Figure 4. The local particle number density, which is zero at the wall and in the mainstream, peaks in the boundary layer closer to the hot wall because it is in the region adjacent to the hot wall for the high activation energy systems, which reaction–nucleation–coagulation phenomena are dominant. This feature has been exploited in our sub-

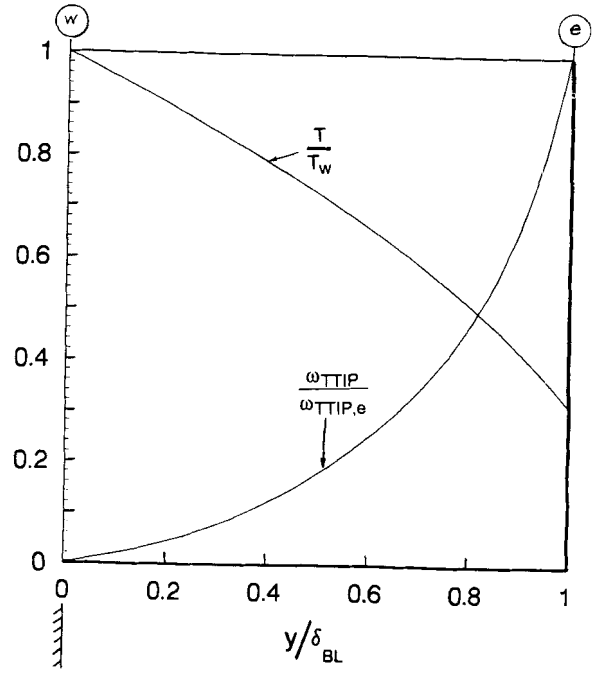

Figure 3. Predicted temperature and TTIP vapor-phase concentration profile.

$T_e = 380$ K, $T_w = 1{,}200$ K.

layer analysis, presented in the subsection on sublayer analysis. In Figure 5 is shown the local particle-size distribution at different locations in the boundary layer. The simultaneous vapor and particle deposition rates can be readily calculated from the calculated vapor concentration and local particle number density (along with local particle-size distribution) in-

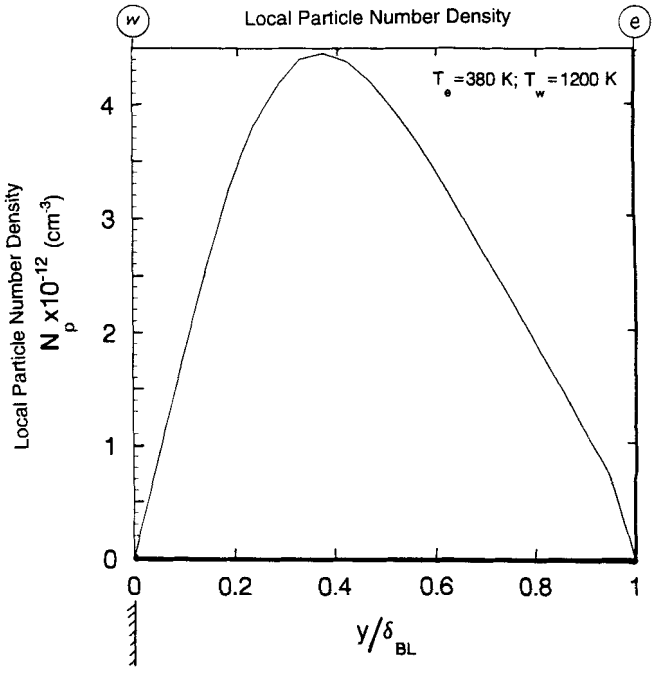

Figure 4. Predicted local particle number densities within vapor boundary layer.

$T_e = 380$ K, $T_w = 1{,}200$ K.

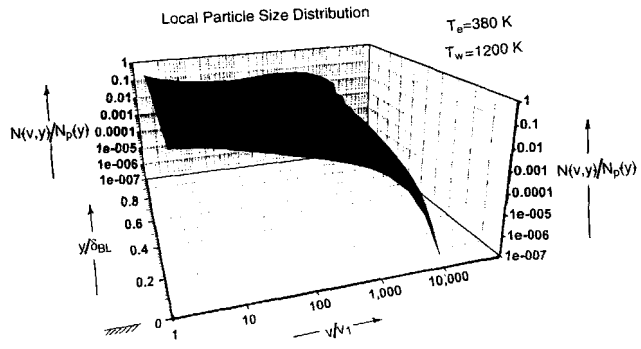

Figure 5. Predicted local particle-size distribution in the boundary layer.

T_e = 380 K, T_w = 1,200 K.

formation. In Figure 6 we compare the results from the present film theory with deposition rates experimentally observed in the impinging jet reactor (Figure 1). Three distinct regimes based on the wall temperatures were observed. Up to a surface temperature of about 700 K, the heterogeneous reaction rate at the wall is the controlling rate process, characterized by a rapid increase in the deposition rate with the wall temperature. Beyond 700 K, the deposition rate is initially external diffusion-controlled and the increase in the deposition rate with the wall temperature is modest. But as the wall temperature is increased beyond 1,100 K, the deposition rate *falls* because of the phenomenon we have termed *vapor phase "ignition"*. This reduction in deposition rate with increasing wall temperature has been attributed to vapor reagent consumption (used in part to generate particles that do not deposit on the surface, and also act as a sink for TTIP vapors by scavenging them). While qualitative agreement is

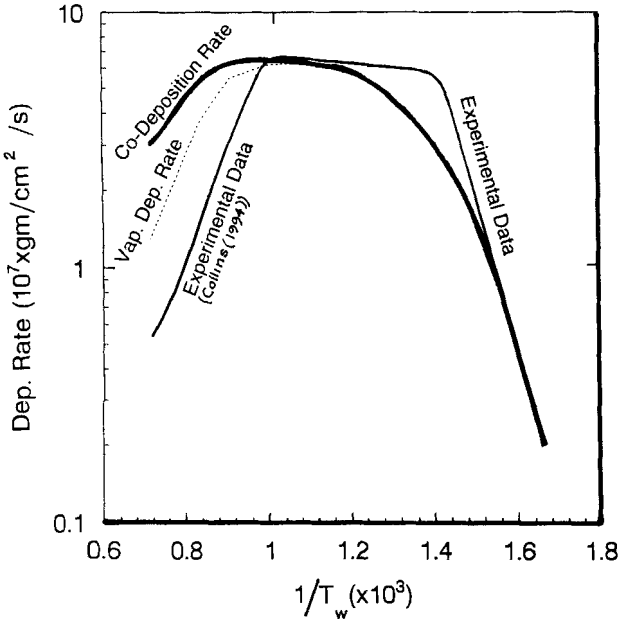

Figure 6. Comparison of vapor and particle deposition rates from film theory and experimentally observed film growth rates in the impinging reactor of Collins (1994).

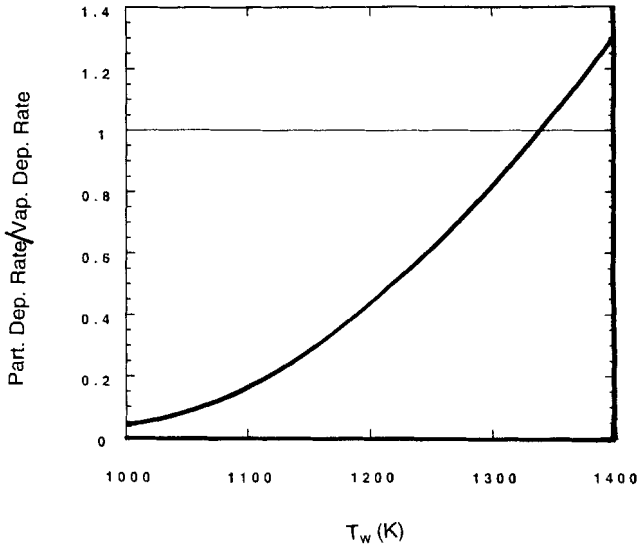

Figure 7. Predicted ratio of particle-to-vapor deposition rates as a function of wall temperature.

observed, the quantitative discrepancy between the experimentally observed and calculated deposition rate results in the post-vapor ignition regime may be a result of the fact that particles in this system are actually aggregates (due to inadequate coalescence rates) and not spherical as considered here. (Our preliminary recalculated results based on aggregate coagulation dynamics and mobility radius (for constant fractal dimension particles) as reported by Rogak and Flagan (1992) are encouraging, but a more comprehensive model that includes finite particle sintering rates will be taken up in our follow-on studies. These methods are now being extended to include laminar counterflow diffusion flows using our recent results on aggregate transport properties and coagulation dynamics (Tandon, 1995; Rosner and Tandon, 1994 [In that article, the relationship between aggregate maximum radius and radius of gyration, Eq. 4, was estimated based on aggregate moment of inertia with respect to one of its axes rather than about its (point) center of mass. Since the latter choice is more relevant, the correct relationship is $R_{max} = R_{gyr}\cdot[D_f + 2)/D_f]^{1/2}$, which does not contain the factor $(3/2)^{1/2}$. No computational results in this article are altered by this change]; Tandon and Rosner, 1995a,b,c). For morphologically complex aggregates, we expect lower film growth rates and better agreement with our experimental data since open aggregated particles provide extra surface area for vapor scavenging and have smaller diffusivities. In Figure 7 are reported relative vapor and particle deposition rates as a function of the wall temperature. As the temperature in the boundary layer increases, a larger fraction of the vapors pyrolize to form particles, resulting in higher particle deposition rates.

Surface roughness and particle/vapor deposition rate

The particle-level simulation methods of Hurt and Allendorf (1991) have illustrated the sensitivity of deposit microstructure to the ratio of particle deposition rate to vapor deposition rate, for example, the surface roughness of deposits is reported as a function of the ratio of particle to vapor deposition rates, which they consider to be a specified

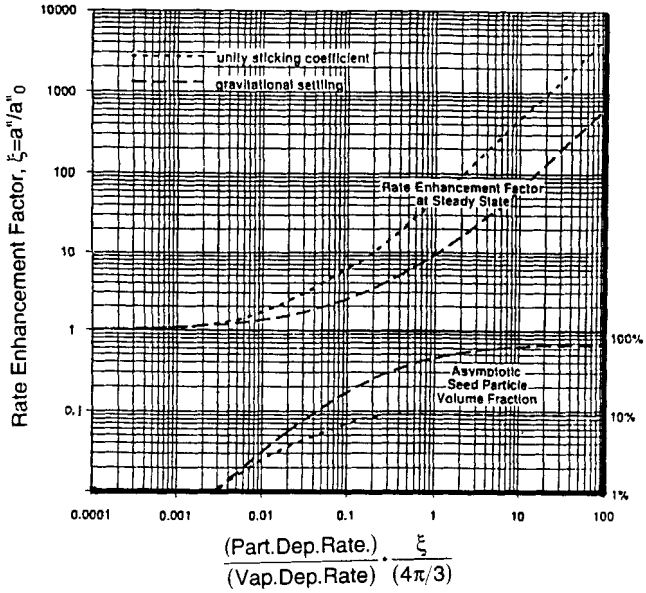

Figure 8. Hurt function showing sensitivity of deposit roughness to the particle/vapor deposition rate ratio; particles of single size following ballistic trajectories.

Courtesy of Hurt and Allendorf (1991) and Allendorf et al. (1993).

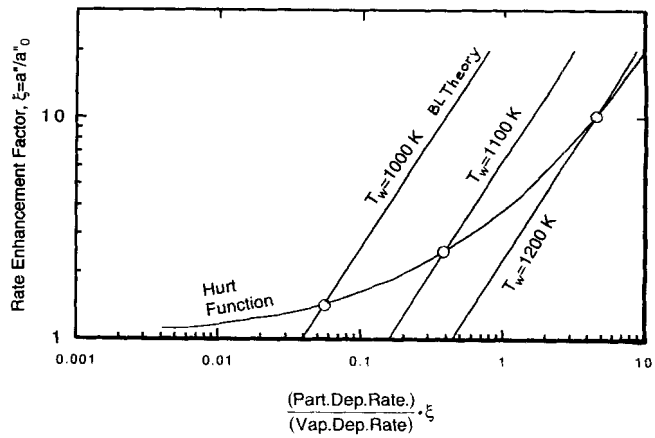

Figure 9. Procedure of self-consistent prediction of vapor and particle deposition rates along with roughness of the resulting deposit.

parameter. The enhancement factors (referred to below as the Hurt function, Figure 8), viewed as the extra interfacial area ($= a''/a_0''$) provided for the heterogeneous reaction because of deposit roughness, give important microstructural information about the deposit. But in systems where there is codeposition by vapors and particles that are themselves generated in the boundary layer, the ratio of particle to vapor deposition rate is not known *a priori* and is, in fact, coupled to the deposition roughness, as illustrated below. A rough deposit provides extra interfacial area for the heterogeneous reaction rate ($\hat{r}_{i,w}'' = (\hat{r}_{i,w}'')_{\text{smooth}} \cdot (a''/a_0'')$), affecting the vapor-phase concentration and local particle number density profiles (because of Eq. 16b). Thus, we see that there is two-way coupling between deposit roughness and ratio of vapor-to-particle deposition rate, and the Hurt function is necessary but not sufficient to predict the steady-state deposition rates along with the corresponding deposit roughness.

This two-way coupling may be dealt with as follows. First we calculate the ratio of particle-to-vapor deposition rates treating surface roughness to be the independent parameter, using the methods discussed in the second section. The results, characterizing the transport aspect of the codeposition process, are then plotted along with the appropriate Hurt function (characterizing microstructure) on the same graph. The point where the two curves intersect provides the steady-state particle and vapor deposition rates and corresponding roughness of the deposit formed (Figure 9).

The Hurt function (Hurt and Allendorf, 1991) in Figure 9 has been calculated for monodispersed particles following ballistic (nondiffusional) trajectories. Therefore their methods/results will need to be generalized to include fine particles with a spectrum of sizes and possessing diffusional motion (Tassopoulos et al., 1988) and are "polydisperse" in size, for making more accurate predictions of deposition rates and self-consistent deposit microstructures. The aim of this study was to semiquantitatively demonstrate the coupling between deposit roughness and ratio of particle/vapor deposition rates and introduce a practical method to predict steady-state vapor and particle deposition rates *along with deposit roughness*.

"Sublayer" analysis of the boundary layer

Castillo and Rosner (1996) recently demonstrated and exploited the existence of a chemical sublayer within the ordinary thermal boundary layer in systems with *high homogeneous activation energy*. As a simplification the overall boundary layer was therefore considered to be divided into two regions: an outer region covering most of the fluid layer where homogeneous chemical reactions were considered "frozen" and a thin inner sublayer (adjacent to the hot surface) where most of the precursor chemistry takes place. Similar ideas applied to CVD systems were proposed and implemented more intuitively by de Croon and Giling (1990). As an extension of chemical sublayer theory of Castillo and Rosner (1996) we here investigate the structure of "reaction–nucleation–coagulation" sublayer inside the ordinary boundary layer.

Vapor-Phase Concentration Profile. The *outer* boundary layer is chemically frozen and the mass balance equation of species i for this quiescent region is

$$0 = -\operatorname{div}\{\boldsymbol{j}_i''\}, \tag{34}$$

where the y-component of the mass flux of species i, $j_{i,y}''$, is given by Eq. 12. The temperature dependence of Fick diffusivity and density have been considered as simple power laws: $D_{i\text{-mix}} \sim T^{n_i}$ and $\rho \sim T^{-1}$, while Soret diffusion factor, α_i, is now considered as nearly constant in the boundary layer. Using the temperature profile in the boundary layer as given by Eq. 3, the local mass balance Eq. 8, a second-order ODE, can be written, using temperature T as the independent variable,

$$T^2 \frac{d^2\omega_i}{dT^2} + T(n_i - 1 - \epsilon - \alpha_i)\frac{d\omega_i}{dT} + \alpha_i \omega_i (n_i + 2 - \epsilon) = 0. \tag{35}$$

Equation 35 admits an analytic solution (Rosner and Tandon, 1991; Schnedler, 1983) given by

$$\omega_{i,\text{outer}}\{T\} = A'T^{\epsilon+2-n} + B'T^{-\alpha}. \tag{36}$$

Since most of the homogeneous chemistry is restricted to the *inner* sublayer, the mass balance equation of species i in this region (Rosner, 1986) is

$$0 = -\operatorname{div}\{\vec{j}_i''\} + \dot{r}_{i,\text{eff}}'''. \tag{37}$$

The second-order differential equation (Eq. 37) is satisfied at each of the M_1 nodes inside the sublayer (node 0 is the edge of the sublayer and M_1+1 is the wall). To solve for the vapor concentration profile in the boundary layer, we solve for M_1+4 variables (mass fraction at each of the M_1 nodes, mass fraction at the wall, mass fraction at the outer edge of the sublayer, and the constants A' and B' appearing in Eq. 36). M_1 equations are obtained by satisfying the finite-difference discretized form of species mass balance equation, Eq. 37, at each of the nodes in the sublayer. Two additional equations are obtained by satisfying the boundary conditions as in Eq. 16. Moreover, at the interface of the outer and inner region the following two matching conditions are satisfied:

$$\omega_{i,\text{outer}} = \omega_{i,\text{inner}} \qquad @\ y = \delta_{SL} \tag{38a}$$

$$j_{i,\text{inner}}'' = j_{i,\text{outer}}'' \qquad @\ y = \delta_{SL}. \tag{38b}$$

Thus we have M_1+4 equations in M_1+4 variables, which are solved simultaneously to obtain the vapor concentration profile of species i in the boundary layer.

Particle Number Density and Size Distribution. A similar approach is extended to predict the local particle number density and particle-size distribution. The boundary layer is again assumed to comprise two regions. In the inner region, adjacent to the wall, processes like coagulation and nucleation are considered to be exclusively restricted. A fraction of particles generated in this region may diffuse through the sublayer to the outer region, while some will diffuse toward the surface. In the outer region, coagulation and nucleation rates are negligible and diffusion is the dominant mechanism. The number density of particles in the ith interval in the outer boundary layer, for no particles in the mainstream, is obtained by solving the PBE, which comprises just the divergence of the diffusion term and is given as

$$N_{i,\text{outer}} = A_i[T^{\epsilon} - T_e^{\epsilon+\alpha_{TP}}T^{-\alpha_{TP}}], \tag{39}$$

where A_i is a constant for size class i. The inner boundary layer is again divided into M_1 nodes. The local particle number densities and size distributions are obtained by satisfying the population balance equation (Eq. 17) at each of the nodes for each of the size interval, i, using methods discussed in the subsection titled "Particle Number Density and Size Distribution," along with the following conditions at the interface of the inner and outer layer:

$$N_{i,\text{inner}} = N_{i,\text{outer}} \qquad @\ y = \delta_{SL} \tag{40a}$$

$$j_{i,\text{inner}}'' = j_{i,\text{outer}}'' \qquad @\ y = \delta_{SL}. \tag{40b}$$

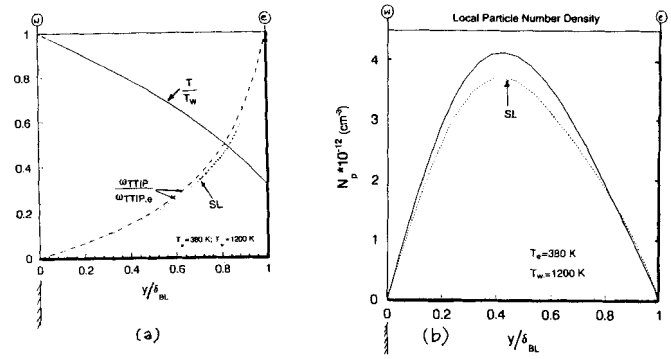

Figure 10. Comparison of sublayer analysis with complete film theory analysis.

Cases shown: (a) temperature and TTIP vapor concentration profile in the boundary layer; (b) total particle number density in the boundary layer.

where $j_{i,\text{inner}}''$ and $j_{i,\text{outer}}''$ are the particle number fluxes in the ith interval in the inner and outer region, respectively. The nucleation–coagulation sublayer thickness, δ_{SL}, has been assumed to be the same as that of the chemical sublayer (of order $\delta_h \cdot (E_{\text{hom}}/RT_e)^{-1} \cdot [\theta_w^2/(\theta_w - 1)]$, where $\theta_w = T_w/T_e$. For the calculations reported here we consider δ_{SL} to be $0.4\delta_{BL}$, a sublayer thickness sufficient for results to be insensitive to the choice of δ_{SL}, and somewhat larger than that obtained from the previously mentioned formula for δ_{CSL}). It is straightforward to calculate vapor and particle flux rates to the surface once local vapor concentration profiles and particle number density and size distributions have been evaluated.

Figure 10 shows results from the sublayer analysis and compare them with calculated results from the complete analysis as outlined earlier. For purposes of comparison, while calculating results from the two methods in Figure 10, the effect of vapor scavenging has been neglected. As can be seen, results from this "sublayer" analysis are in good agreement with the ones obtained from the complete analysis. Accordingly, the strategy for simplification may prove valuable in yet more complex situations.

Defense of Approximations and Generalizations

While the methods developed and illustrated here have been used to demonstrate the essential interactions for this complex class of two-phase transport problems, the present two-phase boundary-layer analysis can now be extended to embrace situations of practical interest with the following added features.

Lewis Number Different from Unity. For Lewis numbers $\{D_i/[k/(\rho c_p)]\}$ different from unity, the thickness of the mass-transfer boundary layer will be different from the thermal boundary layer. Indeed, for the case of TiO_2 film formation from TTIP vapor transport/surface reaction the previously mentioned Lewis number is estimated to be about 0.26, which corresponds to $\delta_m/\delta_h \approx Le^{1/3} \approx 0.64$ (Rosner et al., 1993).

Stagnation-Point Boundary Layer. Real stagnation-point laminar boundary layers, which include true *convection* normal to the hot deposition surface, can be readily incorporated in our one-dimensional model. In dilute reactant CVD systems the solution to the momentum transport equation for

steady, axisymmetric, constant property stagnation point-flow as given by Froessling (Schlichting, 1979) can be used to approximate the velocity field in such a boundary layer, however, no new qualitative features are expected to appear as a result.

Effect of Particle Morphology. To deal with situations where coalescence/restructuring rates are finite or negligible, the coagulation/transport methods illustrated earlier need to be generalized to allow for the presence of morphologically complex aggregates rather than fully coalesced, isolated spherical particles. Current research is focused on fractal aggregate transport properties and coagulation dynamics (Rosner et al., 1991; Tandon, 1995; Tandon and Rosner, 1995a,b; Rosner and Tandon, 1994). The population balance equation, solved here for a single "internal" variable (size) will need to be solved for multi-internal variables (volume, surface area, etc. (Koch and Friedlander, 1990; Xiong and Pratsinis, 1993)).

Homogeneous and Heterogeneous Kinetics. More realistic and, inevitably, more elaborate homogeneous and heterogeneous reaction mechanisms and kinetics may have to be introduced to make adequate predictions of the structure of multiphase boundary layers and resulting deposition rates in some systems.

Nucleation Kinetics. We have assumed (A3) that the vapor precursor TTIP reacts to form TiO_2 molecules that collide (coagulate) and coalesce to condensed TiO_2 particles. This simple nucleation model may prove to be unrealistic even for low vapor pressure products. Appropriate modifications can be included if current research demonstrates that this is necessary and provides a viable alternative approach.

Generation of Hurt Function for a Polydispersed Stream of Particles Following Nonballistic Trajectories. The Hurt function used in the subsection on surface roughness to illustrate our methods for calculating deposition rates and corresponding roughness was derived for mono-sized particles following ballistic trajectories. More generalized functions for a polydispersed mainstream and realistic "arrival/capture" mechanisms will be required to make improved estimates of growth rates and the nature of such "vapor infiltrated" granular films.

These generalizations, beyond the scope of the present work, will be the subject of follow-on investigations motivated, in part, by ancillary experimental results.

Conclusions

To illustrate the complex coupling that exists in CVD situations when particle nucleation and vapor scavenging occur simultaneously we have developed a film theory to predict vapor-phase concentration profiles, associated particle number densities, and size distributions in such nonisothermal boundary layers. We also predict vapor and particle *codeposition rates* on the hot surface and the *associated roughness of the deposit formed.* Thus, we have identified how the deposit surface roughness and deposit microstructure are coupled to the vapor and particle deposition rates, and a self-consistent method has been illustrated to predict codeposition rates and deposit microstructure, taking into account this new level of coupling. For the present illustrative calculations, this theory has been used to predict the growth rate of TiO_2(s) films by *codeposition* of TTIP vapors and TiO_2(s) particles. Anticipating the future need for rational simplifications, we have also carried out an analysis in which a "reaction–nucleation–growth–coagulation" *sublayer* is considered to be embedded well within the ordinary diffusion boundary layer. The existence of this kind of a sublayer is generally limited to nonisothermal systems with high homogeneous activation energy (Rosner et al., 1993; Collins, 1995). Results from this approximate sublayer analysis are shown to be in reasonably good agreement with those obtained from a complete (but more time-consuming) numerical analysis of the boundary layer. Regarding the lack of quantitative agreement with currently available experimental data on deposition rates (Figure 6), we note that particles generated in CVD boundary layers generally have finite-rate or even negligible restructuring (sintering) rates and, as a result, are aggregates rather than fully dense isolated spheres. The model presented here will need to be generalized to include and assess sensitivity to particle morphology. Including particle morphology effects is likely to improve agreement between the predictions and experimental observations because open aggregated particles provide extra surface area for vapor scavenging and have smaller Brownian diffusivities (Rosner and Tandon, 1994; Tandon and Rosner, 1995a).

We believe that the methods discussed here, along with extensions in progress motivated by further comparisons with experimental data, will be useful in controlling the growth rate and morphology of CVD films in situations where particles can be generated in CVD boundary layers. Similar methods will also be useful in systems where particles are deliberately added to modify vapor deposition rates. As part of our longer-range "sol-reaction-engineering" research program, some of the methods here also apply in predicting the structure of multiphase laminar/turbulent flames where aggregates are generated from the vapor phase (Koylu et al., 1995; Xing et al., 1996).

Acknowledgments

It is a pleasure to acknowledge the financial support of US AFOSR (under grant AFOSR 94-1-0143), as well as the related support of the Yale HTCRE Laboratory by our Industrial Affiliates: DuPont, ALCOA. The authors have also benefited from the perceptive comments of Drs. J. Castillo, J. Collins and S. A. Gokoglu.

Notation

$\bar{c}$ = mean thermal speed of molecules
C_{part} = ratio of local heterogeneous reaction rate to local homogeneous reaction rate
d_i = particle diameter associated with $(6v_i/\pi)^{1/3}$
g = gas phase
$G\{r\}$ = radial growth rate
J'' = diffusion number flux
k_B = Boltzmann constant
k_{hom} = homogeneous reaction rate constant
l = gas mean free path
M = molecular weight

Greek letters

β = coagulation rate constant
ϵ = exponent with which gas thermal conductivity scales with temperature
ρ_p = density of an individual particle

Miscellaneous

div{ } = spatial divergence differential operator
(g) = gas (vapor) phase

$\delta(\ )$ = Dirac function
Min $\{p, q\}$ = the lesser of the arguments p and q
(s) = solid phase
$(\ )$ = argument of a function

Literature Cited

Allendorf, M. D., R. H. Hunt, N. Yang, P. Reagan, and M. Robbins, "Deposition of Silicon Carbide Using the Chemical Vapor Composites Process: Process Characterization and Comparison with RASSPVDN Model Predictions," *J. Mat. Res.*, **8**(7), 1651 (1993).

Biswas, P., D. Zhou, I. Zitkovsky, C. Blue, and P. Boolchand, "Superconducting Powders Generated by an Aerosol Process," *Mat. Lett.*, **8**, 233 (1989).

Castillo, J. L., and D. E. Rosner, "Nonequilibrium Theory of Surface Deposition from Particle-Laden, Dilute Condensible Vapor-Containing Streams, Allowing for Particle Thermophoresis and Vapor Scavenging within the Boundary Layer," *Int. J. Multiphase Flow*, **14**(1), 99 (1988).

Castillo, J. L., and D. E. Rosner, "Role of High Activation Energy Homogeneous Chemical Reactions in Affecting CVD-Rates and Deposit Quality for Heated Surfaces," *Chem. Eng. Sci.*, in press (1996).

Collins, J., *Effects of Homogeneous Reaction on the Chemical Vapor Deposition of Titanium Dioxide*, PhD Diss., Dept. of Chemical Engineering, Yale Univ., New Haven, CT (1994).

De Croon, M. H. J. M., and L. J. Giling, "Chemical Boundary Layers in CVD: Part I. Irreversible Reactions," *J. Electrochem. Soc.*, **137**(9), 2867 (1990).

Friedlander, S. K., *Smoke, Dust and Haze*, Wiley, New York (1977).

Garcia-Ybarra, P., and D. E. Rosner, "Thermophoretic Properties of Non-Spherical Particles and Large Molecules," *AIChE J.*, **35**(1), 139 (1989).

Gokoglu, S. A., B. K. Chen, and D. E. Rosner, "Computer Program for the Calculation on Multicomponent Convective Diffusion Deposition Rates from Chemically Frozen Boundary Layer Theory," NASA CR-168329 (1984).

Gomez, A., and D. E. Rosner, "Thermophoretic Effects on Particles in Counterflow Diffusion Flames," *Comb. Sci. Tech.*, **89**, 335 (1993).

Hounslow, M. J., R. L. Ryall, and V. R. Marshall, "A Discretized Population Balance for Nucleation, Growth and Aggregation," *AIChE J.*, **34**(11), 1821 (1988).

Hurt, R. H., and M. D. Allendorf, "Model of Particle-Vapor Codeposition with Application to Ceramic Material Synthesis," *AIChE J.*, **37**(10), 1485 (1991).

Koch, W., and S. K. Friedlander, "The Effect of Particle Coalescence on the Surface Area of a Coagulating Aerosol," *J. Colloid Int. Sci.*, **140**, 419 (1990).

Komiyama, H., and T. Osawa, "Rapid Growth of AlN Films by Particle-Precipitation-Aided Chemical Vapor Deposition," *Jap. J. Appl. Phys.*, **24**, L795 (1985).

Komiyama, H., T. Osawa, H. Kazi, and T. Konno, "Rapid Growth of AlN Films by Particle-Precipitation Aided Chemical Vapor Deposition," *Mat. Sci. Monogr.*, **38A**, 667 (1986).

Komiyama, H., T. Osawa, Y. Shimogaki, N. Wakita, and T. Ueoka, "Particle Precipitation Aided Chemical Vapor Deposition for Rapid Growth of Ceramic Films: Preparation of 1-mm-Thick AlN, TiO_2 and ZrO_2 Films," *Proc. Int. Conf. on Chemical Vapor Deposition*, Electrochemical Soc., Pennington, NJ, p. 1119 (1987).

Koylu, U. O., P. Tandon, Y. Xing, and D. E. Rosner, "Experimental and Theoretical Studies of the Structure of Inorganic Particle Producing Seeded Laminar Counterflow Diffusion Flames," AIChE Meeting, Miami Beach, Paper No. 59p (Nov., 1995).

Okuyama, K., R. Ushio, Y. Kousaka, R. C. Flagan, and J. H. Seinfeld, "Particle Generation in a Chemical Vapor Deposition Process with Seed Particles," *AIChE J.*, **36**(3), 409 (1990).

Okuyama, K., D. Huang, J. H. Seinfeld, N. Tani, and Y. Kousaka, "Aerosol Formulation by Rapid Nucleation of SiO_2 Thin Films from $SiCl_4$ and O_2 Gases by CVD Process," *Chem. Eng. Sci.*, **46**(7), 1545 (1991).

Rogak, S. N., and R. C. Flagan, "Coagulation of Aerosol Agglomerates in the Transition Regime," *J. Colloid Int. Sci.*, **151**(1), 203 (1992).

Rosner, D. E., *Transport Processes in Chemically Reacting Systems*, 3rd printing, Butterworth-Heinemann, Stoneham, MA (1990).

Rosner, D. E., "Thermal (Soret) Diffusion Effects on Interfacial Mass Transport Rates," *J. Physiochem. Hydrodyn.*, **1**, 159 (1980).

Rosner, D. E., and P. Tandon, "Prediction and Correlation of Accessible Area of Large Multiparticle Aggregates," *AIChE J.*, **40**(7), 1167 (1994).

Rosner, D. E., B. K. Chen, G. C. Fryburg, and F. J. Kohl, "Chemically Frozen Multicomponent Boundary Layer Theory of Salt and/or Ash Deposition Rates from Combustion Gases," *Comb. Sci. Tech.*, **20**, 87 (1979).

Rosner, D. E., "Transport Processes and Chemical Kinetics in High Temperature Lamp Modelling," *Proc. Symp. on High Temperature Lamp Chemistry*, Electrochemical Soc., **88-4**, 111 (1988).

Rosner, D. E., J. Collins, and J. L. Castillo, "Onset Conditions for Gas Phase Reactions and Particle Nucleation/Growth in CVD Boundary Layers," *Proc. Int. Symp. on CVD*, Electrochemical Soc., Vol. 93, p. 41 (1993).

Rosner, D. E., and P. Tandon, *Calculations of Na_2SO_4 Chemical Vapor Deposition for Combustion Turbines Running on Coal-Derived Gases*, Yale HTCRE Lab Rep. No. 189 (Sept., 1991).

Rosner, D. E., D. W. Mackowski, M. Tassopoulos, J. L. Castillo, and P. Garcia-Ybarra, "Effects of Heat Transfer on the Dynamics and Transport of Small Particles in Gases," *Ind. Eng. Chem. Res.*, **31**, 760 (1992).

Rosner, D. E., D. W. Mackowski, and P. Garcia-Ybarra, "Size and Structure Insensitivity of the Thermophoretic Transport of Aggregated Soot Particles in Gases," *Comb. Sci. Tech.*, **80**(1–3), 87 (1991).

Schnedler, "Description of Tungsten Transport Processes in Inert Gas Incandescent Lamps," *Phillips J. Res.*, **38**, 224 (1983).

Schlichting, H., *Boundary Layer Theory*, McGraw-Hill, New York (1979).

Shimogaki, Y., and H. Komiyama, "Preparation of Amorphous TiO_2 Films by Thermophoresis-Aided Chemical Vapor Deposition," *Chem. Lett.*, **3**, 267 (1986).

Tandon, P., "Transport Theory for Particles Generated in Combustion Environments," PhD Diss., Dept. of Chemical Engineering, Yale Univ., New Haven, CT (1995).

Tandon, P., and D. E. Rosner, "Translational Brownian Diffusion Coefficient of Large (Multi-Particle) Suspended Aggregates," *Ind. Eng. Chem. Res.*, **34**, 3265 (1995a).

Tandon, P., and D. E. Rosner, "Sintering Kinetics and Transport Property Evolution of Large Multi-Particle Aggregates," *Chem. Eng. Commun.*, in press (1995b).

Tandon, P., and D. E. Rosner, "Self-Preserving Size-Distribution of Populations of Fractal Aggregates Undergoing Brownian Coagulation in the Continuum Regime," (1995c).

Tassopoulos, M., "Relationships Between Particle Deposition Mechanism and Resulting Deposit Microstructure/Effective Transport Properties," PhD Diss., Dept. of Chemical Engineering, Yale Univ., New Haven, CT (1991).

Tassopoulos, M., J. A. O'Brien, and D. E. Rosner, "Simulation of Microstructure-Mechanism Relationships in Particle Deposition," *AIChE J.*, **35**(6), 967 (1988).

Tassopoulos, M., and D. E. Rosner, "Microstructural Descriptors Characterizing Granular Deposits," *AIChE J.*, **38**(1), 15 (1992).

Tassopoulos, M., and D. E. Rosner, "Deposit Roughness for Simultaneous Particle and Vapor Deposition for Polydispersed Mainstream and Non-Ballistic Trajectories," in preparation (1996).

Ulrich, G. D., "Flame Synthesis of Fine Particles," *Chem. Eng. News*, **62**(31), 22 (Aug. 6, 1984).

Waldmann, L., and K. H. Schmitt, "Thermophoresis and Diffusophoresis of Aerosols," *Aerosol Science*, C. N. Davies, ed., Academic Press, New York, p. 137 (1966).

Werner, C., "Modeling of CVD Processes," *Proc. Symp. on Chemical Vapor Deposition*, **93-2**, Electrochemical Soc., p. 48 (1993).

Xing, Y., U. O. Koylu, P. Tandon, and D. E. Rosner, "Measuring and Modelling the Synthesis and Morphological Evolution of Particles in Counterflow Diffusion Flames," World Cong. of Chem. Eng., paper 88d, San Diego (July 14–18, 1996).

Xiong, Y., and S. E. Pratsinis, "Formation of Agglomerate Particles by Coagulation and Sintering: I. A Two-Dimensional Solution of the Population Balance Equation," *J. Aerosol Sci.*, **24**(3), 283 (1993).

Manuscript received July 3, 1995, and revision received Oct. 27, 1995.